PNAS

Supporting Information for

Structure of saguaro cactus virus 3′ translational enhancer mimics 5′ cap for eIF4E binding

Manju Ojha[1], Jeff Vogt[1], Naba Krishna Das[1], Emily Redmond[1], Karndeep Singh[1,2], Hasan Al Banna[1], Tasnia Sadat[1], and Deepak Koirala[1,*]

[1] Department of Chemistry and Biochemistry, University of Maryland Baltimore County, Baltimore, Maryland 21250, USA

[2] Howard Hughes Medical Institute, University of Maryland Baltimore County, Baltimore, Maryland 21250, USA

* Deepak Koirala

Email: dkoirala@umbc.edu

This PDF file includes the following:

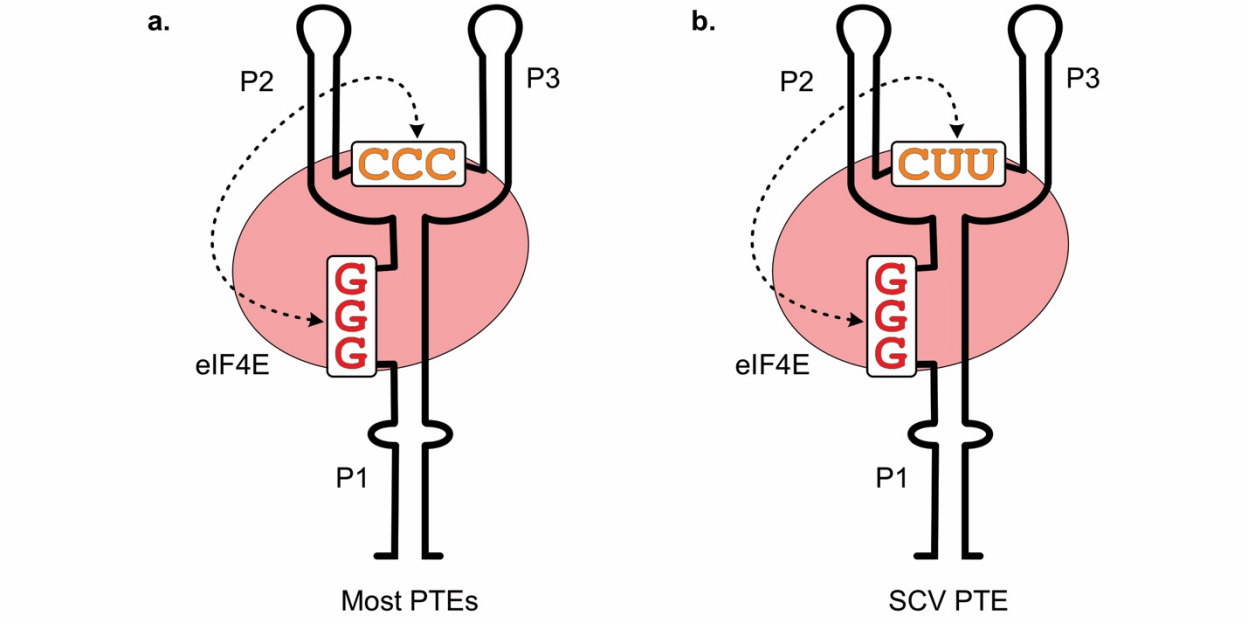

Fig. S1. The schematics of predicted secondary structures of viral PTEs. (a) The representative secondary structure of the PTE found in most plant viruses such as panicum mosaic virus (PMV), pea enation mosaic virus 2 (PEMV2), carnation mottle virus (CarMV), hibiscus chloroticringspot virus (HCRSV), thin paspalum asymptomatic virus (TPAV) and pelargonium flower break virus (PFBV) with G-rich domain (red) and C-rich domain (orange) highlighted (1-3). (b) The secondary structure representation for the SCV PTE with pyrimidine-rich Y and purine-rich R domains are highlighted in orange and red, respectively (4).

Table S1. The RNA and protein sequences used in this study. The crystal structures of the wild-type SCV PTE (G18) and its G18A, G18C, and G18U mutants were determined by Fab-assisted X-ray crystallography.

Construct	Sequence
SCV PTE WT	5'GGUUGCUCGACUGUGAGGGGACCUACCCACUGUGCUGCCACACAGGAACUUCCAACCUUCGGGUGGCGAGGUAGGGCAGAAGAGUGACC
SCV PTE BL3-6	5'GGUUGCUCGACUGUGAGGGGACCUACCCACUGUGGAAACACCACAGGAACUUCCAACCUUCGGGUGGCGAGGUAGGGCAGAAGAGUGACC
SCV PTE G18A mutant	5'GGUUGCUCGACUGUGAGAGGACCUACCCACUGUGGAAACACCACAGGAACUUCCAACCUUCGGGUGGCGAGGUAGGGCAGAAGAGUGACC
SCV PTE G18C mutant	5'GGUUGCUCGACUGUGAGCGGACCUACCCACUGUGGAAACACCACAGGAACUUCCAACCUUCGGGUGGCGAGGUAGGGCAGAAGAGUGACC
SCV PTE G18U mutant	5'GGUUGCUCGACUGUGAGUGGACCUACCCACUGUGGAAACACCACAGGAACUUCCAACCUUCGGGUGGCGAGGUAGGGCAGAAGAGUGACC
6xHis-Wheat eIF4E	MHHHHHHENLYFQGMAHPLENAWTFWFDNPQGKSRQVAWGSTIHPIHTFSTVEDFWGLYNNIHNPSKLNVGADFHCFKNKIEPKWEDPICANGGKWTISCGRGKSDTFWLHTLLAMIGEQFDFGDEICGAVVSVRQKQERVAIWTKNAANEAAQISIGKQWKEFLDYKDSIGFIVHEDAKRSDKGPKNRYTV
6xHis-Human eIF4E	MGHHHHHHSSATVEPETTPTPNPPTTEEEKTESNQEVANPEHYIKHPLQNRWALWFFKNDKSKTWQANLRLISKFDTVEDFWALYNHIQLSSNLMPGCDYSLFKDGIEPMWEDEKNKRGGRWLITLNKQQRRSDLDRFWLETLLCLIGESFDDYSDDVCGAVVNVRAKGDKIAIWTTECENREAVTHIGRVYKERLGLPPKIVIGYQSHADTATKSGSTTKNRFVV
6xHis-***GB1***-Human eIF4E	MGHHHHHHSS***GGMQYKLILNGKTLKGETTTEAVDAATAEKVFKQYANDNGV DGEWTYDDATKTFTVTEIPTTENLYFQGAM***ATVEPETTPTPNPPTTEEEKTESNQEVANPEHYIKHPLQNRWALWFFKNDKSKTWQANLRLISKFDTVEDFWALYNHIQLSSNLMPGCDYSLFKDGIEPMWEDEKNKRGGRWLITLNKQQRRSDLDRFWLETLLCLIGESFDDYSDDVCGAVVNVRAKGDKIAIWTTECENREAVTHIGRVYKERLGLPPKIVIGYQSHADTATKSGSTTKNRFVV
5' capped RNA	5'cap-GGGGUCUCUCUUGUCGAGAGGCAAGGAACCC

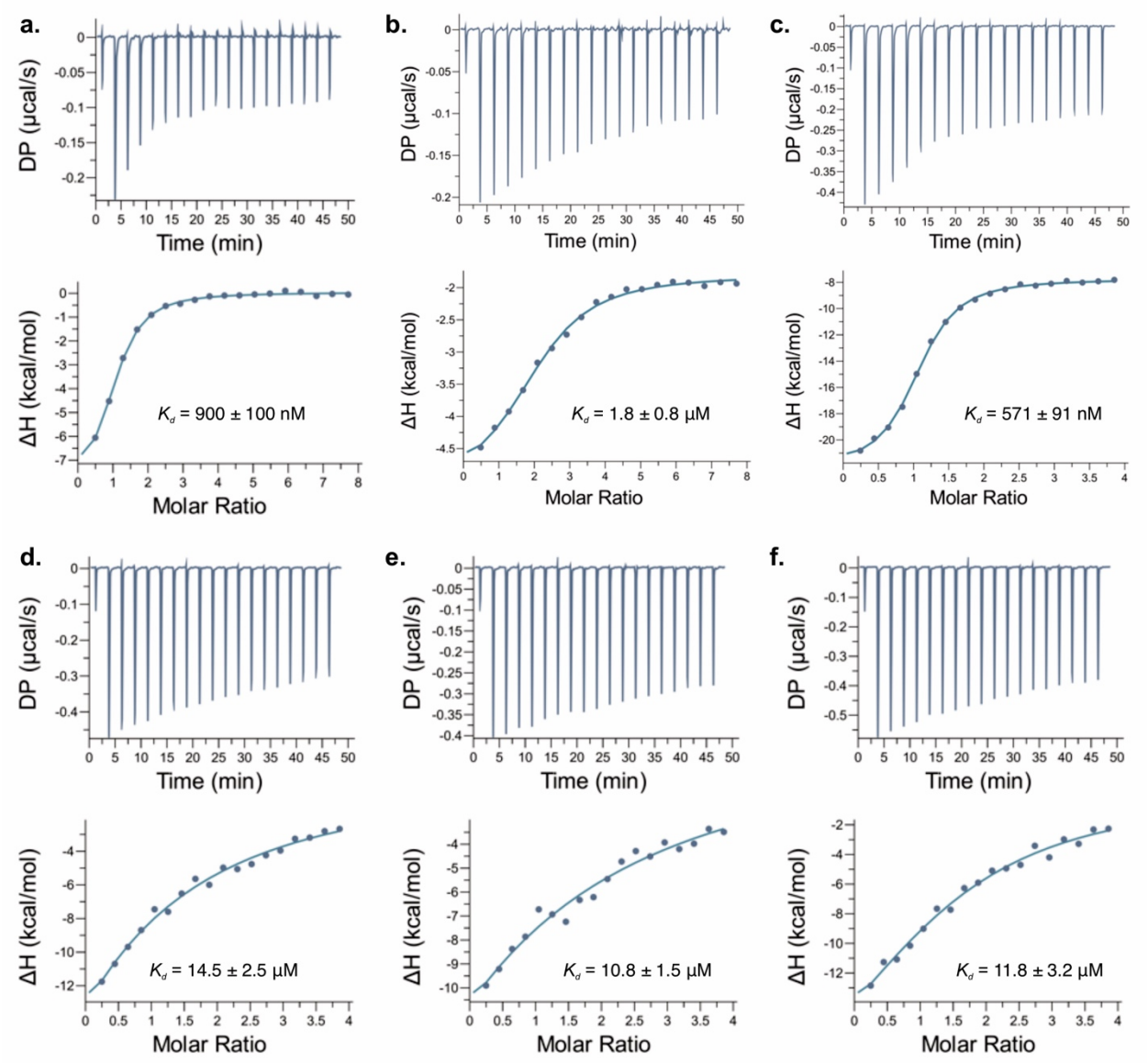

Fig. S2. The ITC measurements for binding interactions of SCV PTE with wheat eIF4E. The representative ITC profiles and corresponding binding curves for (a) the capped RNA, (b) m_7GTP, (c) SCV PTE BL3-6 (d) SCV PTE G18A mutant, (e) SCV PTE G18C mutant, and SCV PTE G18U mutant. The measurements were conducted in the MicroCal PEAQ-ITC (Malvern Panalytical), and data were analyzed using its integrated software. The 19 successive injections of 2 µl of the eIF4E (~100 – 200 µM) from the syringe were made into the RNA (~5 µM) in the calorimetry cell (see methods for details). The reported K_ds are average ± standard deviation values from three (n = 3) separate experiments (see Table S2 below).

Table S2. The results from three replicates of ITC measurements for the SCV PTE binding with wheat eIF4E at 25℃. S.D. stands for standard deviation. Although PTE:eIF4E binding is expected to be 1:1, the deviation of N from 1 perhaps reflects the errors associated with the concentration calculations for the folded protein and RNA (i.e., stacked nucleobases or residues) using the molar extinction coefficients of free nucleotides or residues (i.e., unstacked nucleobases or residues). The active RNA or protein might also be less than the apparent concentration because of the misfolding.

m_7GTP	N (sites)	K_d (M)	ΔH (kcal/mol)	ΔG (kcal/mol)	-TΔS (kcal/mol)
Replicate 1	1.6	1.4×10^{-06}	-3.71	-7.83	4.11
Replicate 2	1.9	2.76×10^{-06}	-11.4	-7.4	4.05
Replicate 3	2.0	1.2×10^{-06}	-20.0	-7.76	12.2
Average ± S.D.	*1.8 ± 0.2*	*(1.8 ± 0.8)* × 10^{-06}	*11.7 ± 8.1*	*-7.6 ± 0.2*	*6.8 ± 4.7*
SCV PTE WT	N (sites)	K_d (M)	ΔH (kcal/mol)	ΔG (kcal/mol)	-TΔS (kcal/mol)
Replicate 1	0.8	6.08×10^{-07}	-10.6	-8.48	2.11
Replicate 2	1.0	2.81×10^{-07}	-13.5	-8.94	4.55
Replicate 3	1.1	6.10×10^{-07}	-24.5	-8.48	16.00
Average ± S.D.	*1.0 ± 0.1*	*(5.0 ± 1.89)* × 10^{-07}	*-16.2 ± 7.3*	*-8.6 ± 0.3*	*7.6 ± 7.4*
SCV PTE BL3-6	N (sites)	K_d (M)	ΔH (kcal/mol)	ΔG (kcal/mol)	-TΔS (kcal/mol)
Replicate 1	1.6	5.93×10^{-07}	-9.66	-8.50	1.17
Replicate 2	1.5	4.71×10^{-07}	-16.8	-8.63	8.21
Replicate 3	1.5	6.49×10^{-07}	-19.0	-8.44	10.6
Average	*1.5 ± 0.0*	*(5.71 ± 0.91)* × 10^{-07}	*-15.1 ± 4.9*	*-8.5 ± 0.1*	*5.3 ± 3.7*
SCV PTE G18A	N (sites)	K_d (M)	ΔH (kcal/mol)	ΔG (kcal/mol)	-TΔS (kcal/mol)
Replicate 1	2.4	13.8×10^{-06}	-40.0	-6.63	33.4
Replicate 2	2.3	17.2×10^{-06}	-48.1	-7.25	40.9
Replicate 3	1.2	12.2×10^{-06}	-37.0	-6.70	30.3
Average ± S.D.	*1.9 ± 0.7*	*(14.5 ± 2.5)* × 10^{-06}	*-41.7 ± 5.7*	*-6.86 ± 0.3*	*34.9 ± 5.5*
SCV PTE G18C	N (sites)	K_d (M)	ΔH (kcal/mol)	ΔG (kcal/mol)	-TΔS (kcal/mol)
Replicate 1	2.19	9.15×10^{-06}	-24.7	-7.11	17.6
Replicate 2	2.25	12.09×10^{-06}	-48.2	-7.22	41.0
Replicate 3	1.63	11.2×10^{-06}	-21.1	-6.77	14.3
Average ± S.D.	*2.0 ± 0.3*	*(10.8 ± 1.5)* × 10^{-06}	*-31.3 ± 14.7*	*-7.0 ± 0.2*	*24.3 ± 14.5*
SCV PTE G18U	N (sites)	K_d (M)	ΔH (kcal/mol)	ΔG (kcal/mol)	-TΔS (kcal/mol)
Replicate 1	2.98	14.1×10^{-06}	-42.8	-6.62	36.2
Replicate 2	2.36	13.16×10^{-06}	-50.8	-7.34	43.5
Replicate 3	1.46	8.23×10^{-06}	-29.6	-6.64	22.7
Average ± S.D.	*2.3 ± 0.8*	*(11.8 ± 3.2)* × 10^{-06}	*-41.1 ± 10.7*	*-6.97 ± 0.4*	*34.1 ± 10.5*

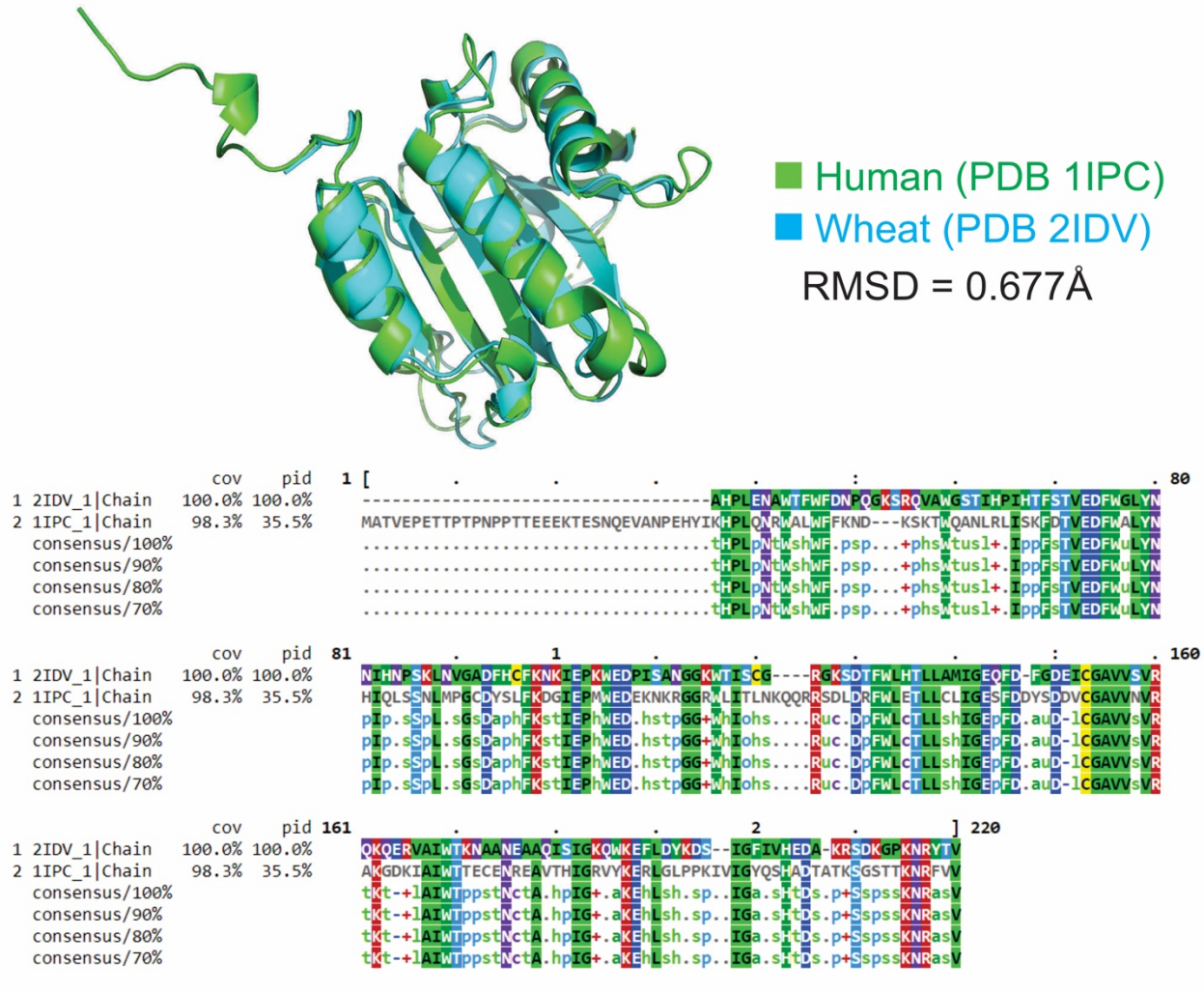

Fig. S3. The superposition of human (green) and wheat (blue) eIF4E crystal structures. Despite having some sequence differences (5) in the human (PDB ID: 1IPC) and wheat (PDB ID: 2IDV), the eIF4Es show a high degree of structural conservation (all-atoms superposition RMSD = 0.677 Å), including the mRNA 5′ cap-binding site.

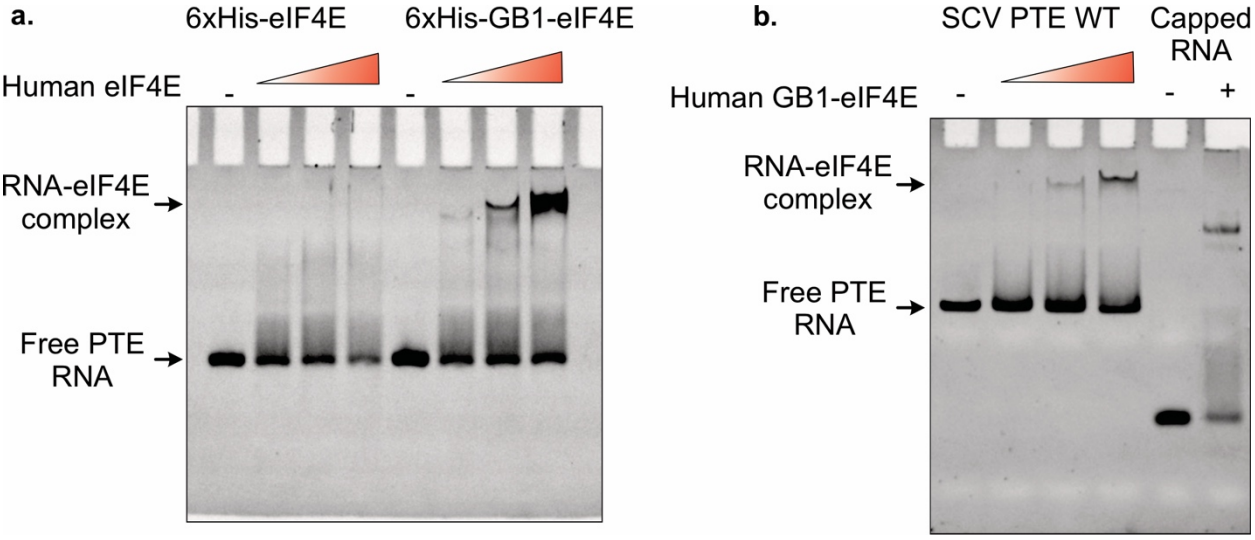

Fig. S4. The native polyacrylamide gel electrophoresis (nPAGE) of the SCV PTE binding with human eIF4E with and without the GB1 domain. (a) The wild-type SCV PTE binding with human eIF4E and GB1-eIF4E showed more defined protein-RNA complex bands with the GB1-eIF4E fusion protein. (b) The wild-type SCV PTE and a capped RNA oligo (different than that used in the gel shown in Figure 1g) binding with the GB1-eIF4E. Each lane was loaded with ~200 ng (~1 μM) of RNA. The eIF4E protein concentration was varied from 4 – 10 μM as indicated by the gradient-filled red triangles. The concentration of GB1-eIF4E used for the capped RNA binding was 10 μM. Although the exact nature of multiple PTE-eIF4E complex bands in EMSA for the capped RNA (also see Figure 1g) is unknown, these bands perhaps reflect the heterogeneity in the RNA and eIF4E conformations. The capped RNA sample is single-stranded and can adopt various conformations, possibly forming multiple secondary structures, some of which might be stabilized by the eIF4E binding with different mobility of the complex in the gel. The GB1-eIF4E protein has a flexible linker between the GB1 and eIF4E domains, allowing sampling of multiple protein conformations with relatively compact or extended forms with potentially different mobilities in the gel. Moreover, the multiple complex bands may be due to the change in eIF4E conformation upon RNA binding as observed previously (6).

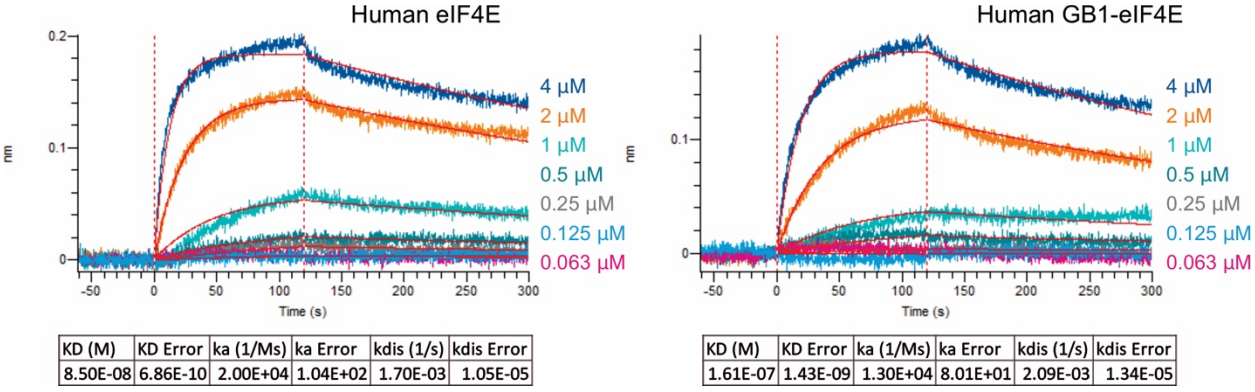

KD (M)	KD Error	ka (1/Ms)	ka Error	kdis (1/s)	kdis Error
8.50E-08	6.86E-10	2.00E+04	1.04E+02	1.70E-03	1.05E-05

KD (M)	KD Error	ka (1/Ms)	ka Error	kdis (1/s)	kdis Error
1.61E-07	1.43E-09	1.30E+04	8.01E+01	2.09E-03	1.34E-05

Fig. S5. The biolayer interferometry (BLI) based kinetics measurements for human eIF4E with and without GB1 domain. The experiments were performed in the Octet R2 system (Sartorius) using the Octet® anti-penta-HIS (HIS1K) biosensors (Sartorius). The His-tagged eIF4E protein (10 µg/ml concentration) was immobilized on the biosensor surface after hydrating the biosensor for 10 minutes in the assay buffer (PBS pH 7.4). These protein-immobilized biosensors were then dipped into varying concentrations of the SCV PTE solution and a reference sample (assay buffer) for the background correction. The data were processed by aligning the baselines and then fitted globally for the association and dissociation steps with the 1:1 protein-RNA binding model using the BLI system-integrated software. The kinetically measured affinities eIF4E and GB1-eIF4E binding were consistent within the same order of magnitude (K_ds = 85 ± 0.7 nM and 161 ± 1.4 nM, respectively) compared to the values measured by the ITC (K_ds = 576 ± 65 nM and 900 ± 236 nM, respectively). However, the kinetics for the association and dissociation steps for GB1-eIF4E protein were slightly slower (k_{on} = 1.3 × 10^4 ± 8.01 $M^{-1}s^{-1}$ and k_{off} = 2.1 × 10^{-3} ± 1.34 × 10^{-5} s^{-1}) than that for eIF4E without the GB1 domain (k_{on} = 2.0 × 10^4 ± 10.4 $M^{-1}s^{-1}$ and k_{off} = 1.7 × 10^{-3} ± 1.05 × 10^{-5} s^{-1}), consistent with the more defined GB1-eIF4E-PTE complex bands in native gel electrophoresis (see Fig. S4).

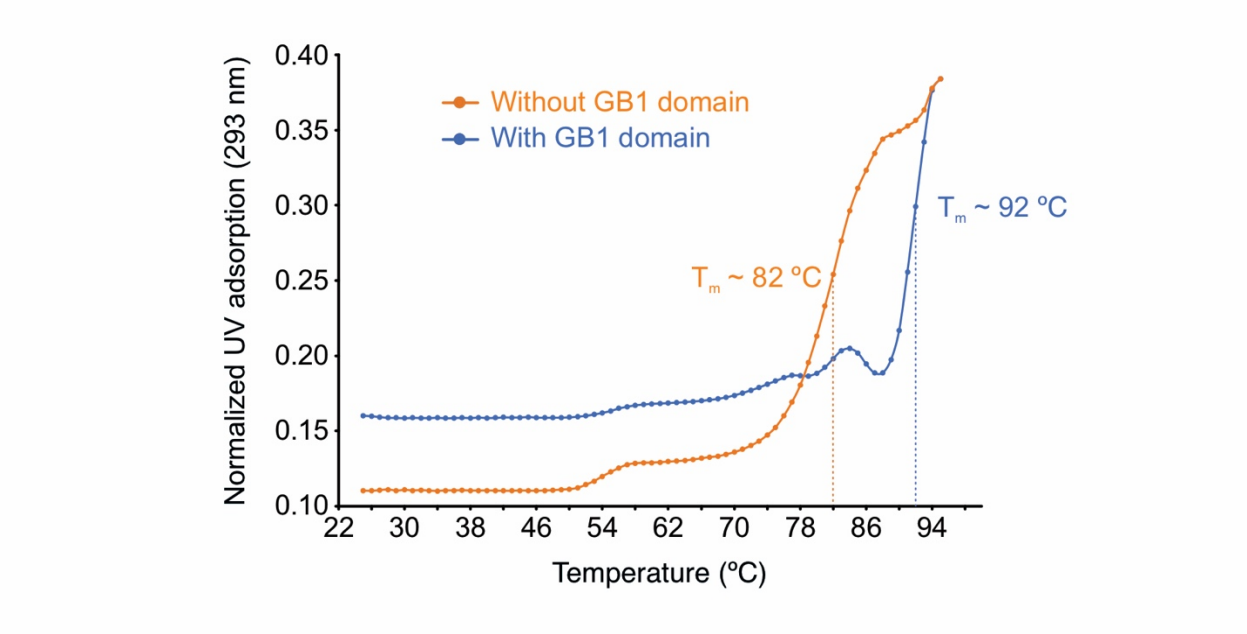

Fig. S6. The UV-melting results for human eIF4E with and without GB1 domain. The experiments were performed in a Carry 3500 UV-spectrophotometer (Agilent Technologies). The protein (5 μM) and reference (PBS buffer, PH 7.4) samples were placed in quartz cuvettes (1 cm path length) side-by-side for the simultaneous measurements. The UV absorptions were recorded at 280, 293, and 600 nm for every 1°C increase in temperature ranging from 25 to 95°C (heating rate = 2°C per minute). The reference absorption at 293 nm and the sample absorption at 600 nm were subtracted to normalize the sample's UV absorption at 293 nm. The normalized UV-absorption at 293 nm as a function of temperature showed about 10°C higher apparent melting temperature for human eIF4E with the GB1 domain (~ 92°C) compared to that for the eIF4E without the GB1 domain (~ 82°C).

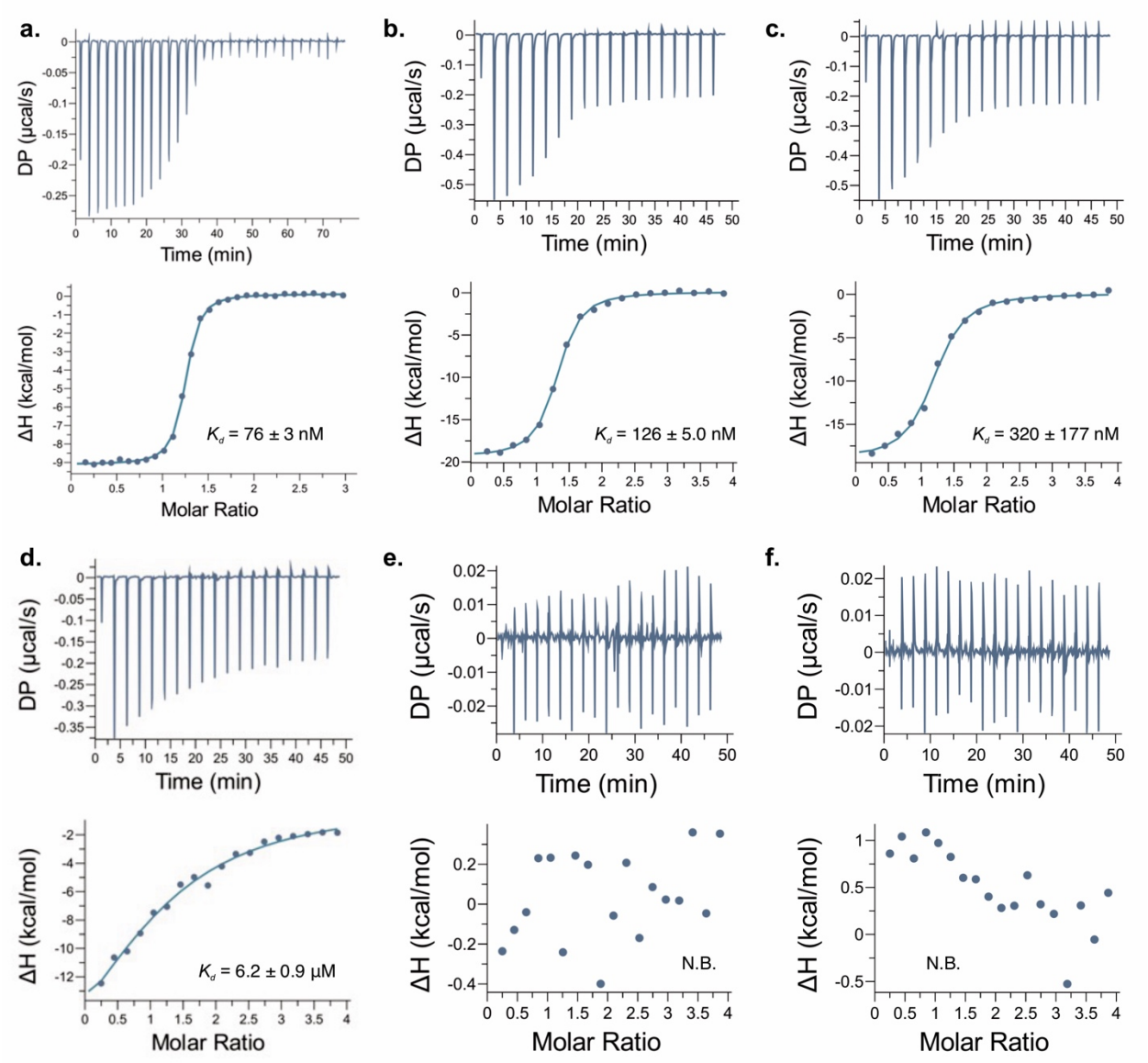

Fig. S7. The ITC measurements for binding interactions of SCV PTE with human eIF4E. The representative ITC profiles and corresponding binding curves for (a) the capped RNA, (b) m_7GTP, (c) SCV PTE BL3-6 (d) SCV PTE G18A mutant, (e) SCV PTE G18C mutant, and (f) SCV PTE G18U mutant. The measurements were conducted in the MicroCal PEAQ-ITC (Malvern Panalytical), and data were analyzed using its integrated software. The 19 successive injections of 2 µl of the eIF4E (~100 µM) from the syringe were made into the RNA (~5 µM) in the calorimetry cell (see methods for details). The reported K_ds are the average ± standard deviation values from three (n = 3) separate experiments, and the N.B. stands for no detectable binding.

Table S3. The results from three replicates of ITC measurements for the SCV PTE binding with human eIF4E at 25°C. S.D. stands for standard deviation. Although PTE:eIF4E binding is expected to be 1:1, the deviation of N from 1 perhaps reflects the errors associated with the concentration calculations for the folded protein and RNA (i.e., stacked nucleobases or residues) using the molar extinction coefficients of free nucleotides or residues (i.e., unstacked nucleobases or residues). The active RNA or protein might also be less than the apparent concentration because of the misfolding.

m_7GTP	N (sites)	K_d (M)	ΔH (kcal/mol)	ΔG (kcal/mol)	-TΔS (kcal/mol)
Replicate 1	2.0	1.21×10^{-07}	-12.8	-9.44	3.39
Replicate 2	1.2	1.30×10^{-07}	-19.3	-9.40	9.89
Replicate 3	1.1	1.26×10^{-07}	-17.4	-9.46	7.96
Average ± S.D.	*1.5 ± 0.5*	*(1.26 ± 0.05)* × 10^{-07}	*-16.4 ± 3.5*	*-9.4 ± 0.03*	*7.1 ± 3.3*
SCV PTE WT	N (sites)	K_d (M)	ΔH (kcal/mol)	ΔG (kcal/mol)	-TΔS (kcal/mol)
Replicate 1	1.0	6.11×10^{-07}	-23.0	-8.45	14.5
Replicate 2	1.0	5.11×10^{-07}	-33.2	-8.58	24.6
Replicate 3	1.1	6.06×10^{-07}	-29.2	-8.47	20.1
Average ± S.D.	*1.0 ± 0.1*	*(5.76 ± 0.56)* × 10^{-07}	*-28.5 ± 5.1*	*-8.5 ± 0.1*	*19.7 ± 5.1*
SCV PTE BL3-6	N (sites)	K_d (M)	ΔH (kcal/mol)	ΔG (kcal/mol)	-TΔS (kcal/mol)
Replicate 1	1.4	5.24×10^{-07}	-12.4	-8.39	4.46
Replicate 2	1.2	2.28×10^{-07}	-18.4	-9.06	9.36
Replicate 3	1.0	2.08×10^{-07}	-18.5	-9.12	8.97
Average	*1.2 ± 0.2*	*(3.2 ± 1.77)* × 10^{-07}	*-16.4 ± 3.1*	*-8.8 ± 0.4*	*7.6 ± 2.7*
SCV PTE G18A	N (sites)	K_d (M)	ΔH (kcal/mol)	ΔG (kcal/mol)	-TΔS (kcal/mol)
Replicate 1	0.6	7.0×10^{-06}	-11.6	-7.03	4.55
Replicate 2	1.2	5.2×10^{-06}	-25.1	-7.21	17.9
Replicate 3	0.6	6.5×10^{-06}	-19.4	-7.65	11.8
Average ± S.D.	*0.8 ± 0.3*	*(6.2 ± 0.9)* × 10^{-06}	*-18.7 ± 6.8*	*-7.3 ± 0.3*	*11.7 ± 6.7*

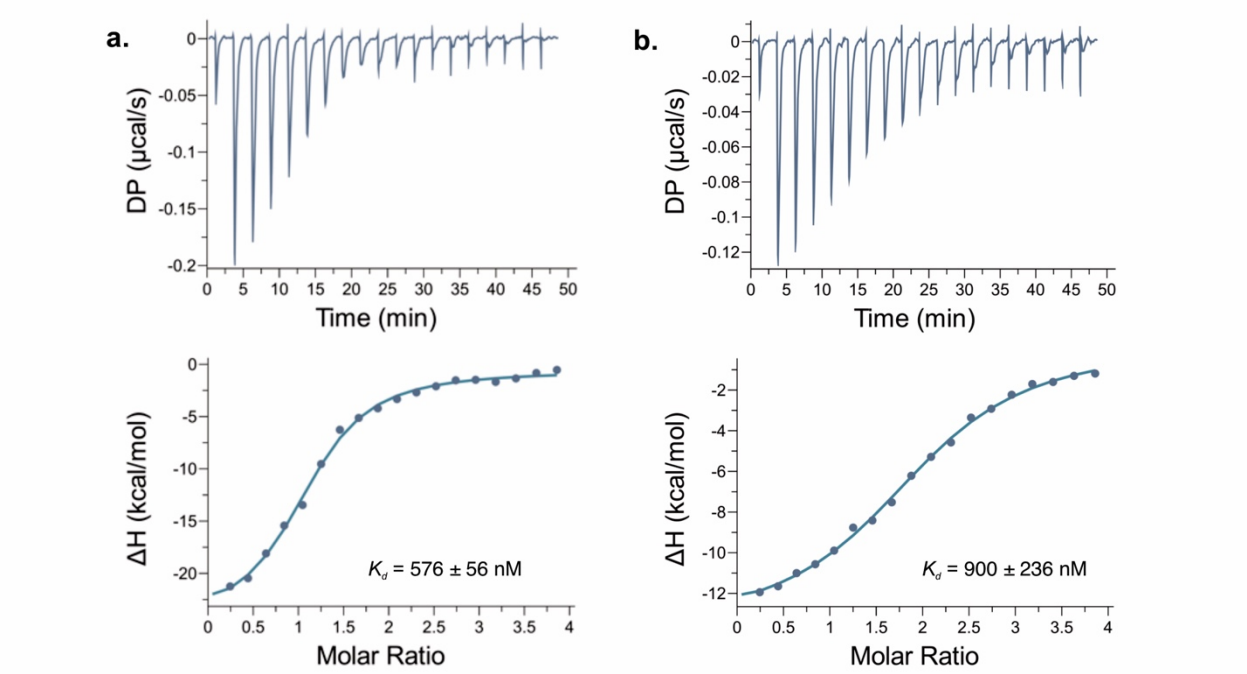

Fig. S8. The ITC measurements for binding interactions of SCV PTE with human eIF4E. The representative ITC profiles and corresponding binding curves for the wild-type SCV PTE with (a) human eIF4E, (a) without, and (b) with GB1 tag fusion. The measurements were conducted in the MicroCal PEAQ-ITC (Malvern Panalytical), and data were analyzed using its integrated software. The 19 successive injections of 2 µl of the eIF4E (~100 µM) from the syringe were made into the RNA (~5 µM) in the calorimetry cell (see methods for details). The reported K_ds are average ± standard deviation values from three (n = 3) separate experiments.

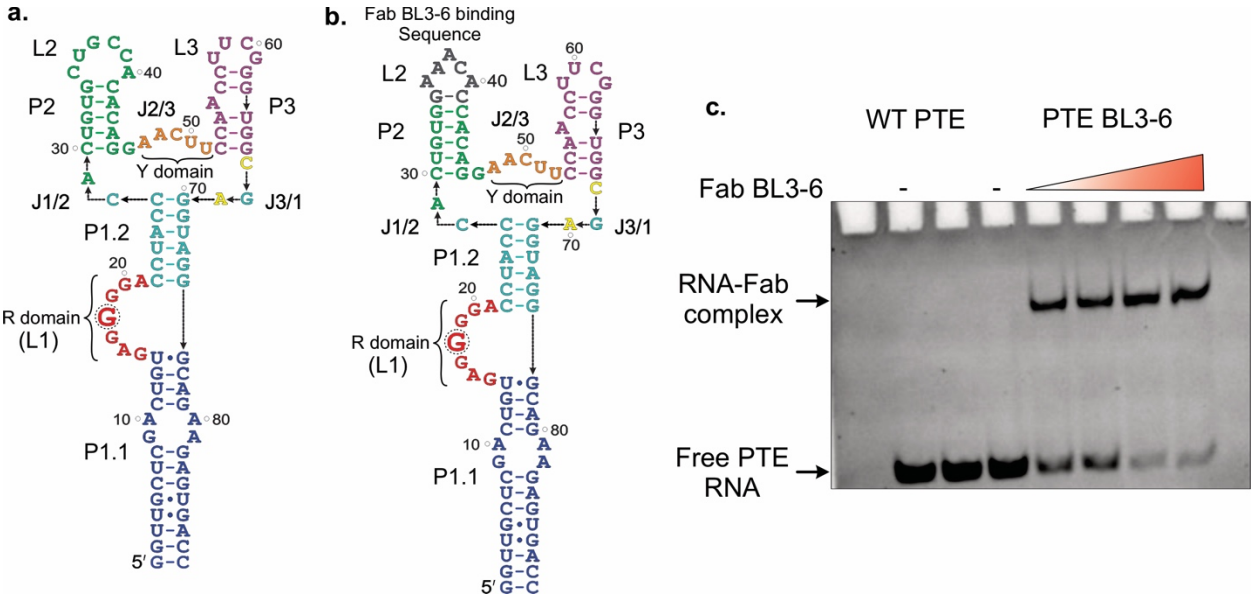

Fig. S9. The binding of Fab BL3-6 with the SCV PTE crystallization constructs. (a) The predicted secondary structure of the wild-type PTE. (b) In the crystallization construct, the Fab BL3-6 binding sequence replaces the L2 loop of the PTE. (c) A native polyacrylamide gel electrophoresis (nPAGE) showing Fab BL3-6 binding with the crystallization construct but not with the wild-type. Each lane was loaded with ~200 ng (~1 μM) of RNA. The Fab concentration was varied from 0.5 – 2 μM as indicated by the gradient-filled red triangles.

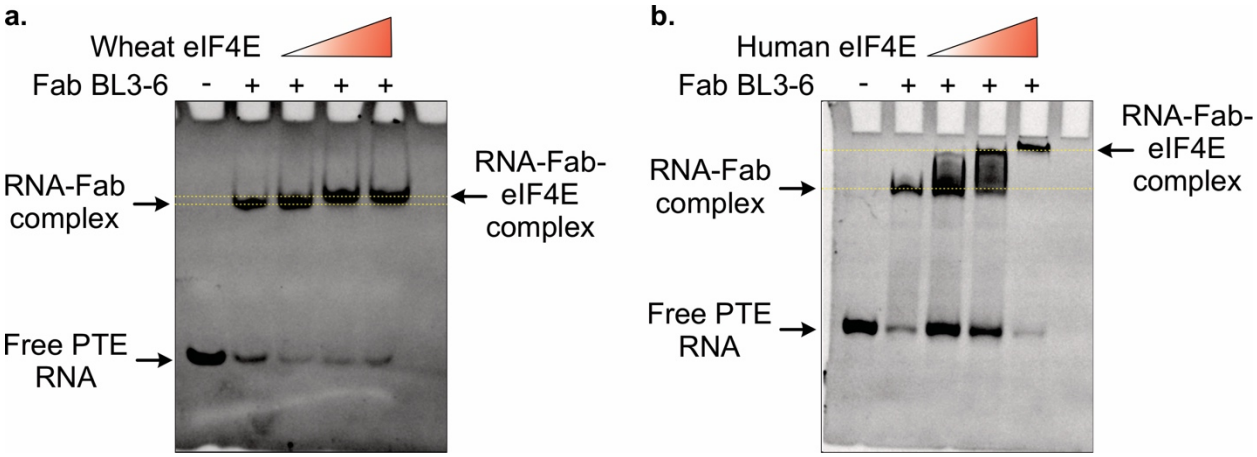

Fig. S10. The binding of eIF4E protein with the PTE crystallization constructs in the presence of Fab BL3-6. The native polyacrylamide gel electrophoresis (nPAGE) for binding of (a) wheat and (b) human eIF4E with the PTE-Fab complex. Each lane was loaded with ~200 ng (~1 μM) of RNA and 1.5 μM of the Fab. The eIF4E protein concentration was varied from 1 – 10 μM as indicated by the gradient-filled red triangles. The dotted yellow lines are for eye guidance.

Table S4. X-ray crystallography data collection and structure refinement statistics. The values in the parentheses are for the highest-resolution shell.

Data collection	***Constructs***			
	SCV PTE (G18)	SCV PTE G18A	SCV PTE G18C	SCV PTE G18U
Space group	I 2 2 2	I 2 2 2	I 2 2 2	I 2 2 2
Resolution (Å)	64.69-3.13 (3.34 – 3.13)	64.3 – 3.17 (3.283 – 3.17)	81.13 – 3.18 (3.294 – 3.18)	64.99 – 3.29 (3.408 – 3.29)
Cell dimensions a, b, c (Å) α, β, γ (°)	77.44, 81.20, 321.20 90.0, 90.0, 90.0	77.37, 80.16, 323.02 90.0, 90.0, 90	77.72, 81.57, 324.50 90.0, 90.0, 90.0	77.77, 81.55, 322.77 90.0, 90.0, 90.0
R_{merge} (%)	5.8 (1.997)	4.1 (2.023)	5.1 (1.588)	4.5 (1.703)
I/σI	14.6 (0.8)	17.2 (0.7)	14.6 (0.9)	18.5 (1.0)
$CC_{1/2}$	0.999 (0.577)	0.999 (0.494)	0.999 (0.510)	1.000 (0.537)
Completeness (%)	99.7 (98.6)	99.9 (100.0)	99.6 (99.6)	99.4 (99.8)
Redundancy	6.6 (6.3)	6.7 (6.5)	6.5 (6.6)	6.8 (7.1)
Refinement				
No. reflections	18416 (3226)	17555 (3108)	17792 (3175)	15976 (3266)
R_{free} (%)	23.26	24.32	24.12	24.32
R_{work} (%)	17.9	18.41	19.77	17.56
R.M.S. deviations				
Bond angles (°)	1.216	1.204	1.311	1.232
Bond length (Å)	0.008	0.008	0.009	0.009
Average B-factor, all atoms ($Å^2$)	127.5	150.2	152.7	151.6
Ramachandran plot of protein residues				
Preferred regions (%)	94.17	93.97	93.50	91.18
Allowed regions (%)	5.83	6.03	6.50	8.12

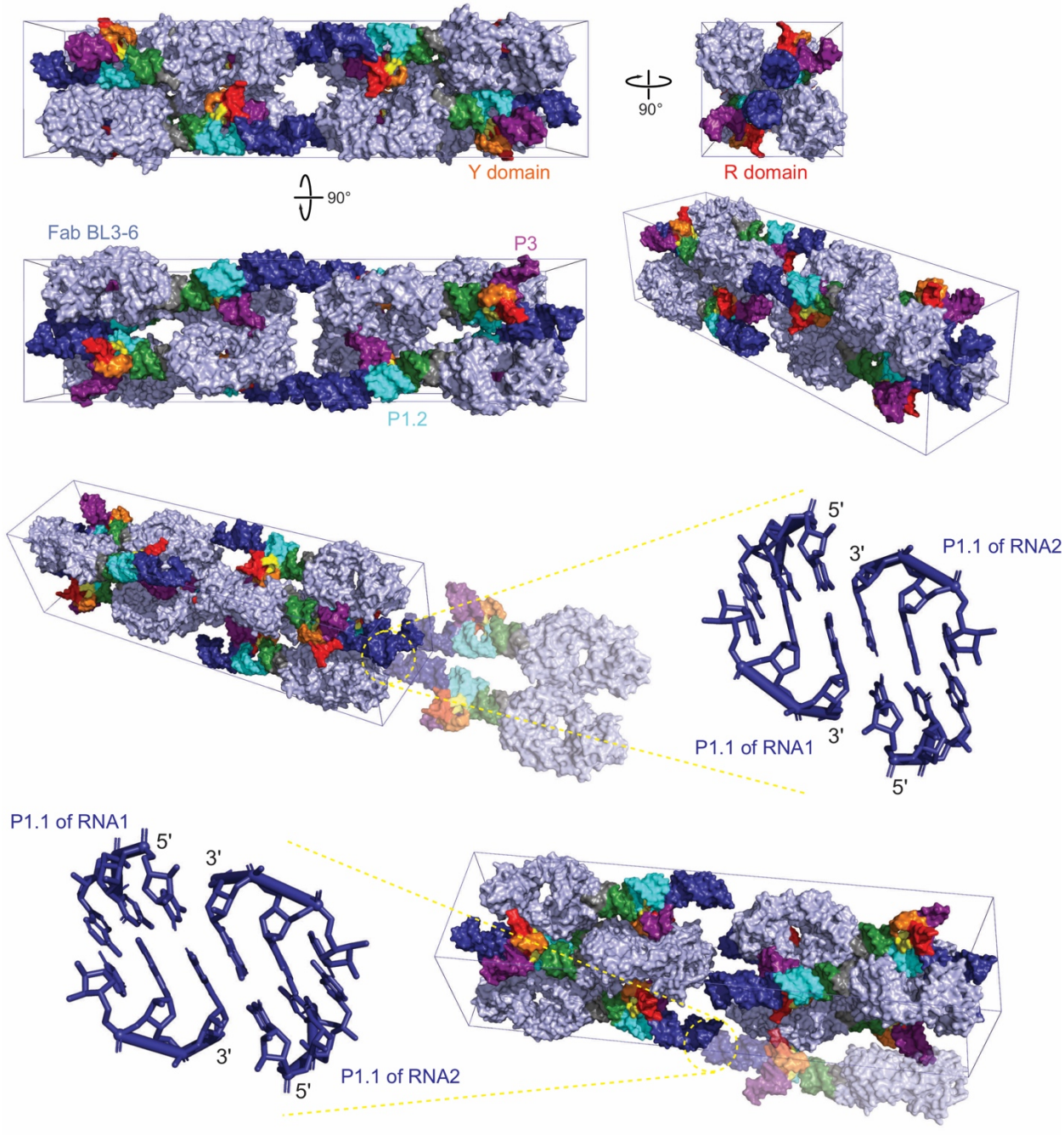

Fig. S11. The Fab-mediated crystal contacts within the crystallographic asymmetric unit. Within the crystal lattice of the PTE-BL3-6 complex, including the Fab-RNA binding interface, the Fab interactions account for about 86.5% of the buried surface area, suggesting a critical role of the Fab in the PTE RNA crystallization. The RNA-RNA interactions involved only the end-to-end stacking of the symmetry-related RNA molecules, accounting for about 13.5% of the buried surface area.

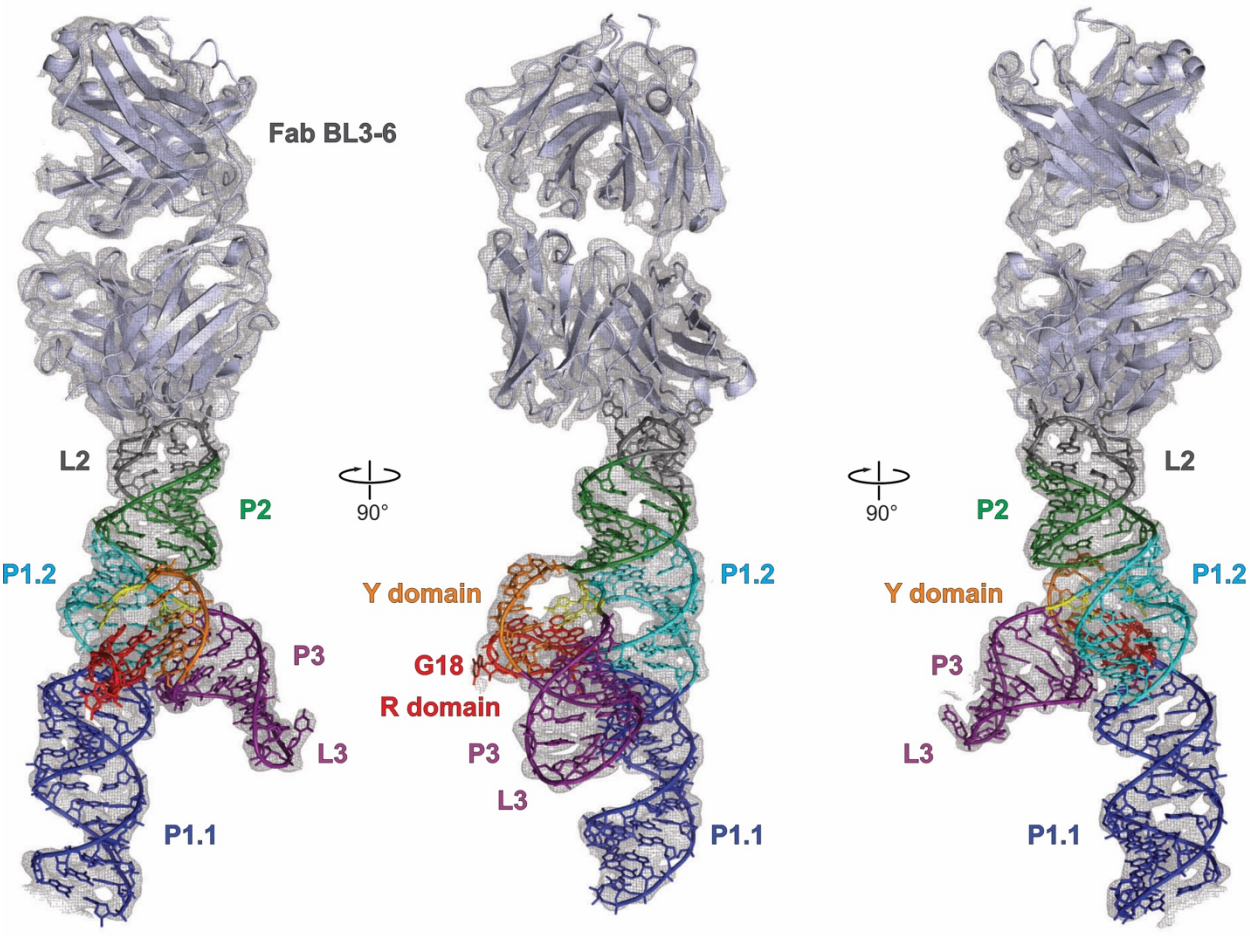

Fig. S12. Overall crystal structure of the SCV PTE in complex with Fab-BL3-6 solved at 3.13 Å resolution. The crystals had a single Fab-RNA complex per crystallographic asymmetric unit. Important features within the structure are labeled. Gray mesh represents the $2|F_o|-|F_c|$ electron density map at contour level 1σ and carve radius 1.8 Å.

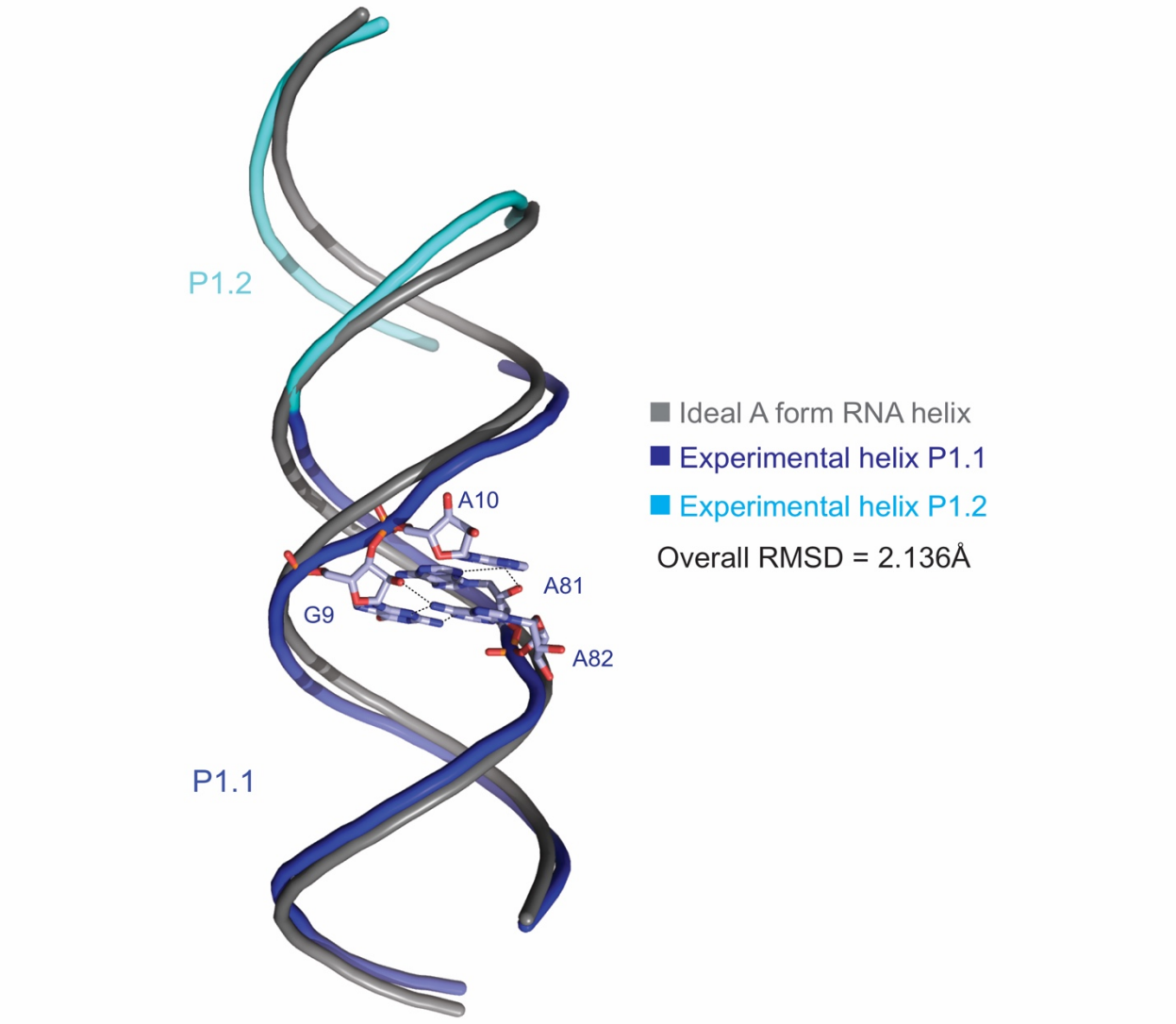

Fig. S13. The superposition of standard A-form RNA helix with the SCV PTE P1 helix that contained non-canonical base pairs (all-atoms superposition RMSD = 2.136 Å). The ideal A-form RNA helix was computed for the same sequence but replaced non-canonical base pairs with canonical ones. Despite the presence of non-canonical pairs, the overall helicity and orientation of the ends for the PTE P1 helix remain very similar compared to the ideal A-form helix.

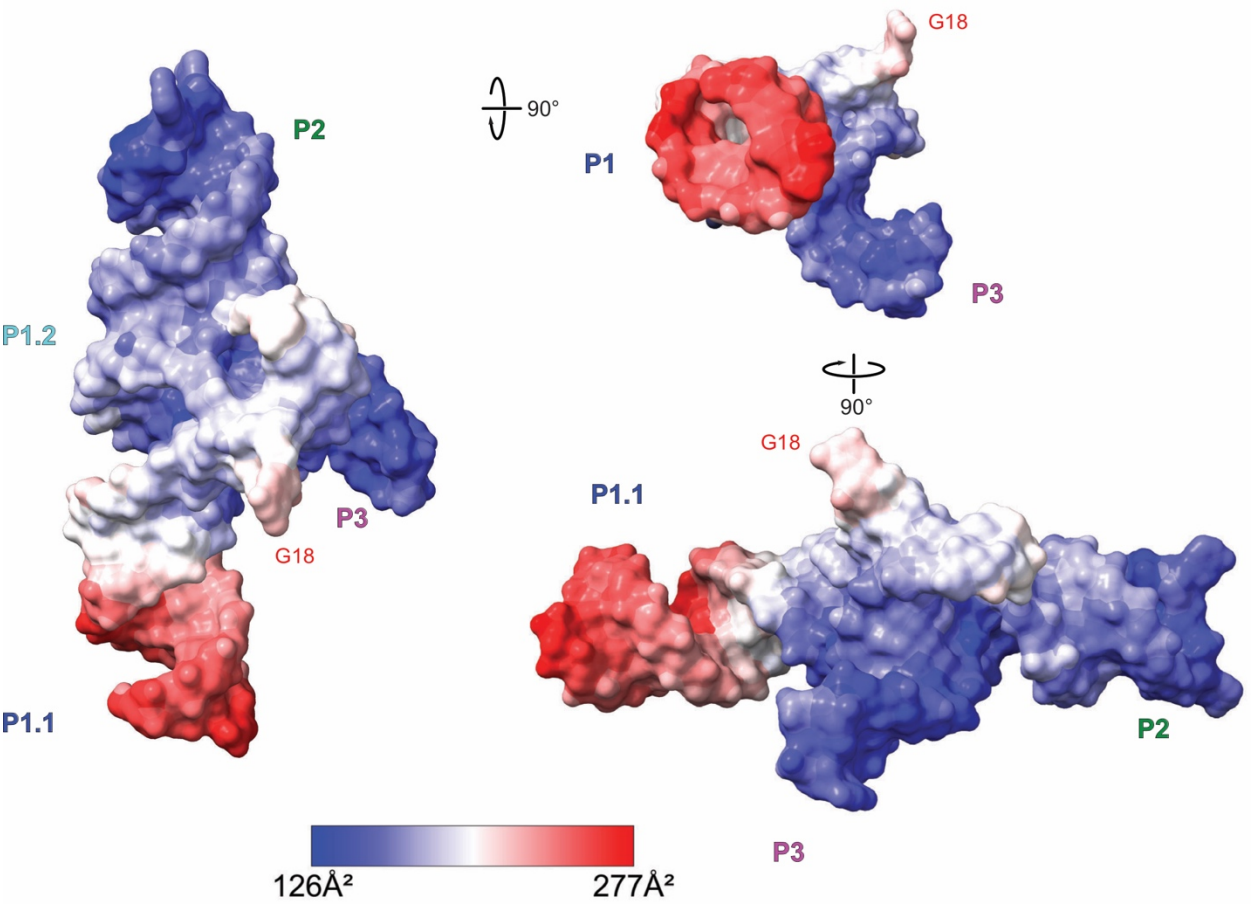

Fig. S14. The crystal structure of the SCV PTE in complex with Fab BL3-6 colored according to the crystallographic B-factors. The gradient from blue to red indicates the structure's lowest (126 $Å^2$) and the highest (277 $Å^2$) B-factors. Notably, the flipped-out G18 has a relatively lower B-factor than some of the based-paired nucleotides within the P1 helix.

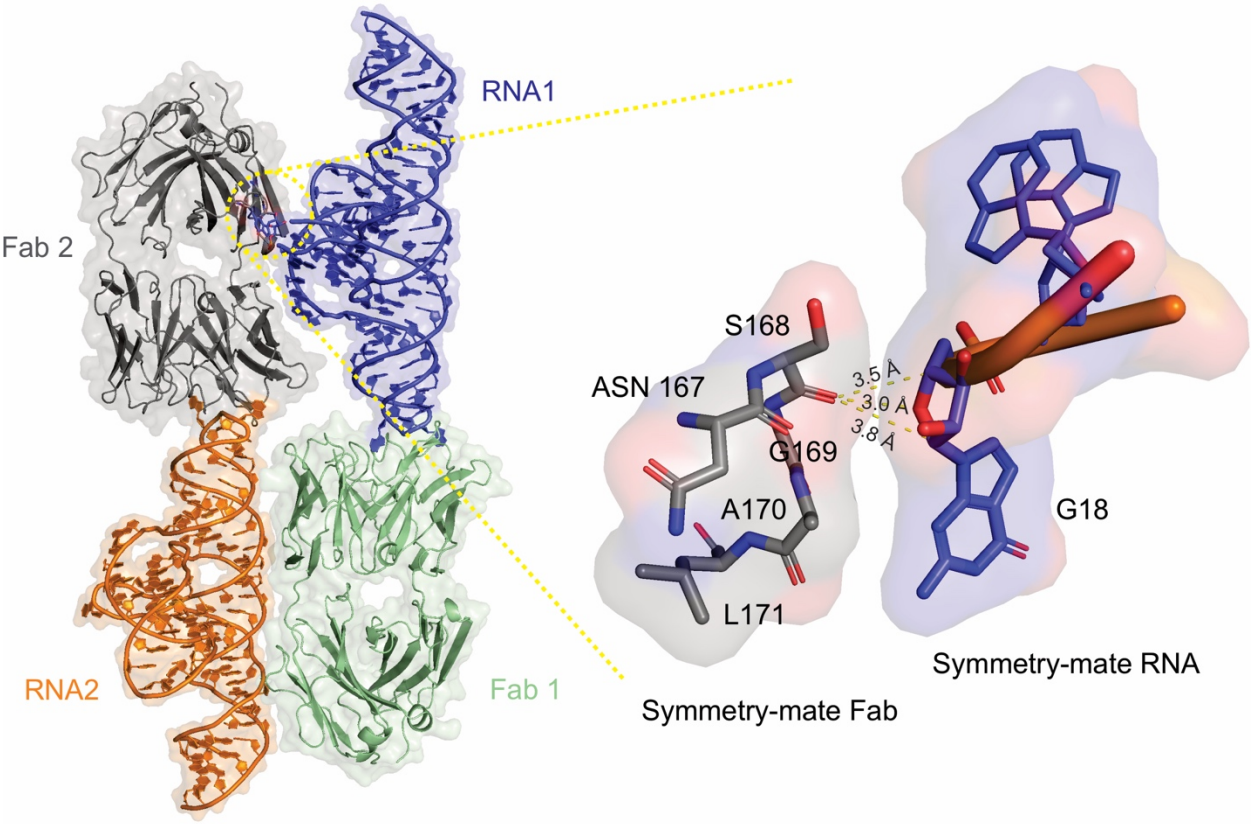

Fig. S15. The crystallographic symmetry-mate Fab residues near the neighboring G18 nucleotide. The nearest distances between the symmetry-related Fab residues to the G18 nucleotide are shown. Although some residues (S168 and A170) of the neighboring Fab molecule in the crystal lattice appear somewhat near the G18 nucleotide (≥ 3 Å), these contacts do not correspond to the direct hydrogen bonding interactions.

Materials and methods

RNA synthesis and purification. The RNA constructs for this study were synthesized by *in vitro* transcription. DNA templates with a T7 promoter sequence for the transcription reaction were produced by PCR amplification of ssDNA purchased from Integrated DNA Technologies (IDT). The first two nucleotides of reverse primer were 2′ OMe modified to reduce the 3′ end heterogeneity of the transcript (7). The transcription reaction was conducted for 3 hours at 37 °C in a buffer containing 40 mM Tris-HCl, pH 8.0, 2 mM spermidine, 10 mM NaCl, 25 mM $MgCl_2$, 1 mM DTT, 40 U/ml RNase inhibitor, 5 U/ml TIPPase, 5 mM of each NTP, 50 pmol/ml DNA template, and 50 μg/ml homemade T7 RNA polymerase (8). The reaction was then quenched by adding 10 U/ml DNase I (Promega) and incubating at 37°C for 1 hour. All RNA samples were purified by denaturing polyacrylamide gel electrophoresis (dPAGE). The RNA band was visualized by UV shadowing, excised from the gel, crushed, and eluted overnight at 4 °C in 10 mM Tris, pH 8.0, 2 mM EDTA, and 300 mM NaCl. The buffer of eluted RNA was exchanged with pure water three times using a 10 kDa cut-off Amicon column (Millipore Sigma). RNA was collected, aliquoted into 300 μl fractions, and stored at -80°C until further use.

Fab expression and purification. The Fab BL3-6 expression plasmid was a kind gift from Joseph Piccirilli, the University of Chicago. The Fab was expressed and purified according to published protocols (9-11). Briefly, the plasmid was transformed into 55244 *E. coli* competent cells and streaked into an LB-agar plate with 100 μg/ml of carbenicillin. Several colonies were selected to inoculate a 15 ml starter culture and grown at 30°C for 8 hours. The starter culture was then used to inoculate 1 liter of 2xYT media, and cells were grown for 24 hours at 30°C. For Fab overexpression, the cells were centrifuged at 22°C and 6000g for 10 minutes, resuspended in 1-liter phosphate-depleted media, and grown for 24 hours at 30°C. The cells were harvested by centrifugation at 4°C and 6000g for 10 minutes, resuspended in PBS, pH 7.4 buffer with 0.01 mg/ml bovine pancreas DNase I (Sigma-Aldrich), and 400 mM Phenylmethylsulfonyl fluoride (PMSF), and lysed by sonication (Qsonica, Cole-Parmer). The mixture was first centrifuged at 18000 rpm, the clear lysate was filtered through a 0.45-micron filter (VWR), and the Fab was purified using the Bio-Rad NGC fast protein liquid chromatography (FPLC) system. First, the lysate was passed through a Hi-trap protein A column (Cytiva), and the captured Fab was eluted with 0.1 M acetic acid. The fractions were collected, diluted using PBS pH 7.4 buffer, and loaded

into a Hi-trap protein G column (Cytiva). The eluted Fab fractions from the protein G column in 0.1 M glycine, pH 2.7, were collected, diluted with a 50 mM NaOAc, 50 mM NaCl, pH 5.5 buffer, and loaded into a Hi-trap heparin column (Cytiva). Finally, the Fab fractions eluted from the heparin column by the gradient elution using 50 mM NaOAc, 2 M NaCl, and pH 5.5 buffer were collected, and buffer was exchanged 3 times with PBS pH 7.4 using 30 kDa cut-off Amicon column (Millipore Sigma). The concentrated Fab was collected, analyzed by 12% SDS-PAGE, and tested for RNase activity using the RNaseAlert kit (Ambion, www. thermofisher.com). The aliquots (~300 µl) of purified Fab were stored at -80 °C.

Human and wheat eIF4E expression and purification. The human and wheat eIF4E genes were cloned into a pET-16b (+) vector (GenScript, https://www.genscript.com) with a 6x-His tag at the N-terminal. The expression plasmid for the GB1 tag fused human eIF4E was a generous gift from Prof. Michael Summers. The plasmids were transformed into BL21 (DE3) E. coli. The bacterial culture was grown into LB supplemented with 100 µg/ml of ampicillin at 37 ℃ with 220 rpm in a 5 ml starter culture for 6 hours, which was then used to inoculate 1L culture for overnight growth. The protein overexpression was induced using IPTG to the final concentration of 0.5 mM for 4 hours at 25 ℃ before harvesting the bacteria through centrifugation at 6000 g for 10 minutes at 4 ℃. The cell pellets were then resuspended using lysis buffer (50 mM Tris-base, 500 mM NaCl, and 20 mM imidazole) and lysed using sonication. The lysate was centrifuged at 18000 rpm at 4°C, and the supernatant was passed through a 0.45-micron filter. The clarified lysate was then applied to a 5 ml HisTrap™ column (Cytiva), and the protein was eluted from the column isocratically with a buffer (50 mM Tris-base, 500 mM NaCl, 250 mM imidazole) after washing the column with 5 column volumes of the lysis buffer. The eluted fractions were collected, diluted with PBS buffer pH 7.4 for human eIF4E and with 50 mM HEPES, 5 mM $MgCl_2$, 100 mM KCl, and 5% glycerol for wheat eIF4E and purified further by size-exclusion chromatography (HiLoad® 26/600 Superdex® 200 pg column, Cytiva). The single-peak protein fractions were pooled and concentrated using the Amicon centrifugal filters (molecular weight cut-off 10 kDa, Millipore Sigma) and stored at -80°C.

5′ capped RNA synthesis and purification. The 5′ capped RNA oligomer was synthesized and purified according to the previously reported protocols (12, 13). Briefly, about 20 µM of a 5′ triphosphate uncapped RNA in water was heated at 90°C for 3 minutes and snap-cooled on ice,

followed by the addition of an appropriate volume of a capping buffer (50 mM Tris-base pH 8.0, 5 mM KCl, 1 mM MgCl2, and 1 mM DTT) supplemented with 1 mM GTP, 0.2 mM S-adenosyl methionine (SAM), and a vaccinia virus capping enzyme. The reaction mixture was incubated at 37 °C for 2 hours and then quenched by adding 250 mM EDTA pH 8.0 and heating at 90°C for 5 minutes, and snap-cooling on ice., The capped RNA was purified by dPAGE and stored at -80 °C.

Native gel electrophoresis assay. About 200 ng RNA in water was refolded in a buffer containing 10 mM Tris-HCl, pH 7.4, 5 mM $MgCl_2$, and 300 mM NaCl. For refolding, the RNA was heated at 90°C for 1 minute, and an appropriate volume of the refolding buffer was added, followed by incubation at 50°C for 10 minutes and in ice for 5 minutes. The refolded RNA was then incubated for 30 minutes at room temperature with different Fab or eIF4E protein equivalents. The protein-RNA complex samples were mixed with an appropriate volume of native gel loading solution that contained 30% glycerol, 0.1% bromophenol blue, and xylene cyanol. These samples were loaded onto 10% native polyacrylamide gels for human eIF4E while 5% native polyacrylamide gels for wheat eIF4E and run at 115 V in pre-cooled 0.5x TBE buffer (50 mM Tris-base, 50 mM boric acid, and 1 mM EDTA, pH 7.5) at 4°C. The gels were stained with ethidium bromide and imaged using the Azure 200 gel documentation system (Azure Biosystems).

Isothermal titration calorimetry. The isothermal titration calorimetry (ITC) experiments were carried out in the MicroCal PEAQ-ITC automated equipment (Malvern Panalytical) using freshly prepared RNA and protein samples. For wheat eIF4E, the RNA and protein samples were dialyzed overnight with a buffer containing 50 mM HEPES, pH 7.6, 100 mM KCl, 5 mM $MgCl_2$, and 5% glycerol. For human eIF4E, the RNA and protein samples were dialyzed overnight with PBS pH 7.4 buffer containing 5 mM $MgCl_2$. The injection syringe contained 150 µl of 100 µM of human or 200 µM of wheat eIF4E protein, and the calorimetry cell was loaded with 500 µl of 5 µM RNA. After thermal equilibration at 25°C and an initial 60-second delay, a single injection of 0.2 µl followed by the 19 serial injections of 2 µl of the protein was made into the calorimetry cell. The reported K_d for each RNA construct represents the average ± standard deviation obtained from at least triplicate independent measurements.

Crystallization. The RNA sample (~ 600 µg) was refolded in a refolding buffer containing 10 mM Tris-HCl, pH 7.4, 5 mM $MgCl_2$, and 300 mM NaCl as described above for the native gel electrophoresis assay. The refolded RNA was then incubated for 30 min at RT with 1.1 equivalents

of the Fab and concentrated to 6 mg/ml using a 10-kDa cut-off, Amicon Ultra-1 column (Millipore Sigma). Then, Fab−RNA complexes were passed through 0.2 μm cut-off Millipore centrifugal filter units (www.emdmillipore.com). The Xtal3 Mosquito liquid handling robot (TTP Labtech, ttplabtech.com) was used to set up hanging-drop vapor-diffusion crystallization screens at room temperature (22°C) within a humidity-controlled (70%) chamber using commercially available screening kits from Hampton Research. The crystals were observed within a week, mainly in two conditions. Using the hanging drop vapor diffusion method, these initial hit conditions were further optimized for pH, precipitant, and salt concentration to grow larger crystals. The crystals grew to full size within a week. Drops containing suitable crystals were brought up to 40% glycerol for cryoprotection without changing the other compositions. The crystals were immediately flash-frozen in liquid nitrogen after being fished in the loops from the drops and taken to Argonne National Laboratory for X-ray diffraction screening and data collection.

Crystallographic data collection, processing, and analysis. The X-ray diffraction data sets were collected at the Advanced Photon Source NE-CAT section beamlines 24-ID-C and 24-ID-E. All the datasets were then integrated and scaled using its on-site RAPD automated programs (https://rapd.nec.aps.anl.gov/rapd/). The initial phases were obtained by molecular replacement with the previously reported structure of Fab BL3-6 (PDB code: 8DP3) (14) as the search model using Phaser on Phenix (15). Iterative model building and refinement were performed using the COOT (16) and the Phenix package (15). The RNA structure was built unambiguously by modeling the individual nucleotides into the electron density map obtained from the molecular replacement. The refinement used default NCS options and auto-selected TLS parameters in Phenix. The solvent-accessible surface area and buried surface area for the crystal lattice interactions were calculated using PDBePISA (http://www.ebi.ac.uk/pdbe/pisa/) (17). The structure-related figures were made in PyMOL (The PyMOL Molecular Graphics System, Version 2.0 Schrödinger, LLC), and the figure labels were edited in CorelDraw (Corel Corporation, http://www.corel.com).

Molecular docking source code

The following Python-based script was used to perform the molecular docking studies of human and wheat eIF4Es with the SCV PTE crystal structure (see methods for details).

```
from pymol import cmd, stored
import random
cmd.load("input.pdb")
cmd.center("input & c. E & i. 18 & n. C2+C4+C6") #Center the view on the Guanine 18
aromatic ring
max_rot = 10.0 #Maximum rotation is +/- 5 degrees
for x in range(1, 1000): #This is the number of output models for each pass.
    name = "out_%03d" % x #Name the output file based on the iteration
    cmd.copy(name, "input")
    chain = "%s & c. E" % name
    cmd.center("%s & c. E & i. 18 & n. C2+C4+C6" % name) #Re-Center view after last move
    x = (random.random() * max_rot) - 5
    y = (random.random() * max_rot) - 5
    z = (random.random() * max_rot) - 5
    cmd.rotate("X", x, chain)
    cmd.rotate("Y", y, chain)
    cmd.rotate("Z", z, chain)
    filename = ".\\%s.pdb" % name
    cmd.save(filename, name)
    cmd.delete(name)
```

SI References

1. J. S. Batten, B. Desvoyes, Y. Yamamura, K.-B. G. Scholthof, A translational enhancer element on the 3′-proximal end of the Panicum mosaic virus genome. *FEBS Letters* **580**, 2591-2597 (2006).
2. J. J. Kraft *et al.*, The 3' Untranslated Region of a Plant Viral RNA Directs Efficient Cap-Independent Translation in Plant and Mammalian Systems. *Pathogens* **8** (2019).
3. A. E. Simon, W. A. Miller, 3′ Cap-Independent Translation Enhancers of Plant Viruses. *Ann. Rev. Microbiol.* **67**, 21-42 (2013).
4. M. Chattopadhyay, K. Shi, X. Yuan, A. E. Simon, Long-distance kissing loop interactions between a 3' proximal Y-shaped structure and apical loops of 5' hairpins enhance translation of Saguaro cactus virus. *Virology* **417**, 113-125 (2011).
5. A. F. Monzingo *et al.*, The structure of eukaryotic translation initiation factor-4E from wheat reveals a novel disulfide bond. *Plant Physiol* **143**, 1504-1518 (2007).
6. L. Volpon, M. J. Osborne, I. Topisirovic, N. Siddiqui, K. L. Borden, Cap-free structure of eIF4E suggests a basis for conformational regulation by its ligands. *The EMBO Journal* **25**, 5138-5149 (2006).

7. C. Kao, S. Rüdisser, M. Zheng, A simple and efficient method to transcribe RNAs with reduced 3′ heterogeneity. *Methods* **23**, 201-205 (2001).
8. D. C. Rio, Expression and Purification of Active Recombinant T7 RNA Polymerase from E. coli. *Cold Spring Harb. Protoc.* **2013**, pdb.prot078527 (2013).
9. J.-D. Ye *et al.*, Synthetic antibodies for specific recognition and crystallization of structured RNA. *Proc. Natl. Acad. Sci. U.S.A.* **105**, 82-87 (2008).
10. Y. Koldobskaya *et al.*, A portable RNA sequence whose recognition by a synthetic antibody facilitates structural determination. *Nat Struct Mol Biol* **18**, 100-106 (2011).
11. M. Paduch *et al.*, Generating conformation-specific synthetic antibodies to trap proteins in selected functional states. *Methods* **60**, 3-14 (2013).
12. J. D. Brown *et al.*, Structural basis for transcriptional start site control of HIV-1 RNA fate. *Science* **368**, 413-417 (2020).
13. P. Ding *et al.*, 5'-Cap sequestration is an essential determinant of HIV-1 genome packaging. *Proc Natl Acad Sci U S A* **118** (2021).
14. N. K. Das *et al.*, Crystal structure of a highly conserved enteroviral 5' cloverleaf RNA replication element. *Nat Commun* **14**, 1955 (2023).
15. P. D. Adams *et al.*, PHENIX: a comprehensive Python-based system for macromolecular structure solution. *Acta Crystallogr. D* **66**, 213-221 (2010).
16. P. Emsley, B. Lohkamp, W. G. Scott, K. Cowtan, Features and development of Coot. *Acta Crystallogr D Biol Crystallogr* **66**, 486-501 (2010).
17. E. Krissinel, K. Henrick, Inference of macromolecular assemblies from crystalline state. *J. Mol. Biol.* **372**, 774-797 (2007).